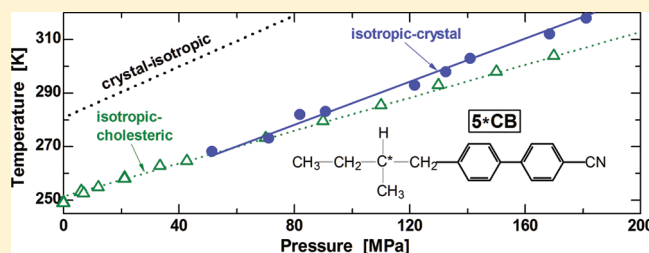


# Phase Diagram and Dynamics of the Liquid Crystal Isopentylcyanobiphenyl (5\*CB)

D. Fragiadakis,<sup>†</sup> S. Urban,<sup>‡</sup> M. Massalska-Arodz,<sup>§</sup> R. B. Bogoslovov,<sup>†,||</sup> J. Czub,<sup>‡,⊥</sup> and C. M. Roland<sup>\*,†</sup><sup>†</sup>Chemistry Division, Naval Research Laboratory, Code 6120, Washington, DC 20375-5342, United States<sup>‡</sup>Institute of Physics, Jagiellonian University, Kraków, Poland<sup>§</sup>Institute of Nuclear Physics, Polish Academy of Sciences, Kraków, Poland

**ABSTRACT:** From measurements of the specific volume as a function of temperature and pressure, the phase diagram for the liquid crystal forming isopentylcyanobiphenyl (5\*CB) was determined. There are a number of phases (isotropic liquid, glass, cholesteric, and crystalline), and we show that the phase boundaries differ from previous reports, reflecting the slow crystallization kinetics of the system. Using dielectric spectroscopy at ambient and elevated pressure, we identify the relaxation processes in the isotropic and cholesteric phases. From application of density scaling to the dynamics, we obtain scaling exponents, which were found to vary with the type of motion. Moreover, unlike previous results for many other liquid crystals, the scaling exponent for the isotropic state differs from the thermodynamic potential parameter, and hence the relaxation time along the clearing line varies significantly with pressure. The distinctive properties of 5\*CB reflect the very different volume dependences of the thermodynamics and the dynamics.



## INTRODUCTION

The *n*-alkyl and *n*-alkoxy cyano-biphenyl compounds were synthesized in 1972 by Gray et al.,<sup>1</sup> and since that time they have become the most intensively studied liquid crystalline (LC) substances. Among them, the 4-pentyl-4'-cyanobiphenyl (5CB), used in early liquid crystal displays, has special significance. 5CB has a simple chemical structure, a convenient range of temperatures for the nematic phase (18–35 °C), chemical, light, and thermal stability, and a strong dipole moment, facilitating dielectric measurements. Its chiral (right-handed) counterpart, 4-(2-methylbutyl) 4'-cyanobiphenyl (or isopentylcyanobiphenyl, 5\*CB; see Figure 1), was synthesized in 1976 by the same group.<sup>2</sup> At room temperature, 5\*CB exists in the isotropic phase, with an interesting polymorphism revealed by various experiments,<sup>2–8</sup> as summarized in the phase diagram (Figure 1) showing schematically the temperature dependence of the free energy of various phases:<sup>7</sup> (i) a monotropic system of phases with stable isotropic and crystalline phase I, (ii) a metastable cholesteric phase and its glass, and (iii) a metastable disordered crystalline phase II and its glass. Both glassy phases can be attained with slow cooling (1 K/min). On heating 5\*CB from low temperature, a softening of the glass to the metastable cholesteric phase occurs, followed by transition to the supercooled isotropic phase. Crystallization is achieved only by first cooling the sample to the glass of the cholesteric phase and then heating above the cholesteric–isotropic liquid phase transition.<sup>4</sup> Subsequent isothermal crystallization requires about 2 h.

5\*CB has interesting dielectric properties.<sup>3,4,9,10</sup> Phase transitions observed by other methods are clearly seen in the change in static permittivity with temperature, and dielectric relaxation

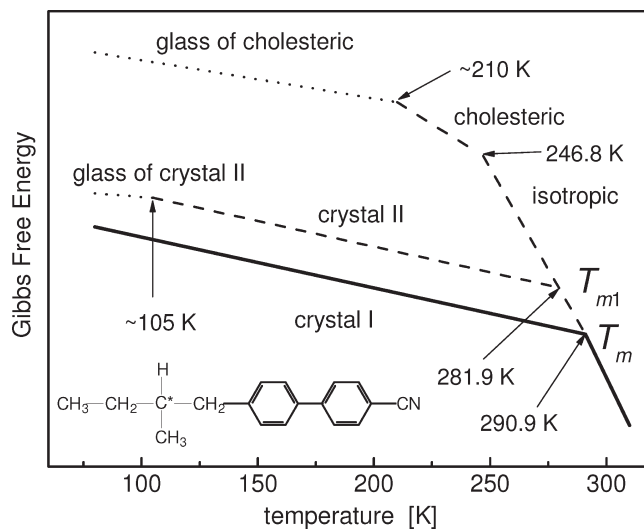


**Figure 1.** Schematic phase diagram of Gibbs energy versus temperature for isopentylcyanobiphenyl (5\*CB, structure shown), based on adiabatic calorimetry studies at ambient pressure.<sup>6,7</sup> Solid lines are for stable phases, dashed are for metastable phases, and dotted are for glasses. The observed transition temperatures are noted.

shows the influence of temperature<sup>3,4,9</sup> and pressure<sup>10</sup> on the dynamics in the isotropic, cholesteric, and glassy phases. The

**Received:** March 2, 2011

**Revised:** April 11, 2011

**Published:** May 03, 2011

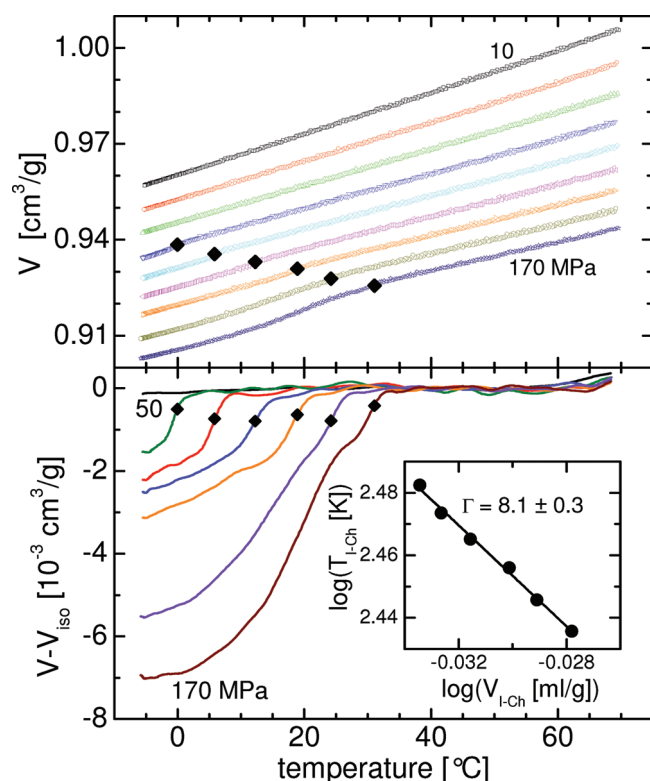


**Figure 2.** (top) Specific volume versus temperature for 5\*CB during isobaric cooling at pressures from 10 to 170 MPa in steps of 20 MPa. The “◆” denote the isotropic–cholesteric transition on cooling. (bottom) Specific volume versus temperature after subtraction of a linear fit to the isotropic state volume and smoothing, with the I–Ch transition indicated by “◆”. A sharp decrease in volume on cooling, corresponding to the isotropic–cholesteric transition, is evident. The additional, larger and more gradual decrease in the scans at 150 and 170 MPa at lower temperatures is due to crystallization. The inset is a double logarithmic plot of the temperature and specific volume at the transition indicated by the “◆” in the main graph.

structural relaxation time  $\tau_\alpha$  characterizing molecular rotations in the isotropic and supercooled cholesteric liquids follows the empirical Vogel–Fulcher–Tammann–Hesse (VTFH) equation.<sup>11</sup> The non-Arrhenius behavior of  $\tau_\alpha$  is observed more than 100 K above vitrification, unlike the behavior of 5CB in the isotropic phase.<sup>9</sup>

The present study of 5\*CB had two main aims: to establish the phase diagram in a broad range of temperature,  $T$ , and pressure,  $P$ , together with the equation of state,  $V(P, T)$ , and to measure the dielectric relaxation times at different thermodynamic conditions in the isotropic and cholesteric phases. From these data, we apply the thermodynamic scaling of  $\tau$ , as has been done for many glassformers (ref 12 and references therein) and liquid crystals (ref 13 and references therein). This provides information about the steepness of the interaction potential, which in turn can be compared to the thermodynamic potential parameter quantifying the relative effect of volume and temperature on the phase transition.<sup>14</sup>

## EXPERIMENTAL SECTION

Pressure–volume–temperature (PVT) measurements employed a Gnomix instrument.<sup>15</sup> The change in specific volume was measured as temperature was decreased at 0.5 K/min in the

range 263–343 K at various fixed pressures up to 200 MPa. The absolute density was measured at ambient conditions using the buoyancy method.

Dielectric relaxation spectroscopy (DRS) was carried out using cylindrical electrodes (15 mm diameter) with a 0.2 mm Teflon spacer inserted to maintain constant thickness. Spectra were obtained with a Novocontrol Alpha analyzer ( $10^{-2}$ – $10^6$  Hz) and an IMASS time domain dielectric analyzer ( $10^{-4}$ – $10^3$  Hz). For ambient pressure measurements, the temperature was controlled using a Delta Design model 9023 oven. For elevated pressure measurements, the sample capacitor assembly was contained in a Manganin cell (Harwood Engineering) placed in a Tenney Jr. chamber (temperature control was  $\pm 0.1$  K at the sample). The sample capacitor was protected from contamination from the surrounding medium by flexible seals. The pressure was applied using a hydraulic pump (Enerpac) in combination with a pressure intensifier (Harwood engineering). Pressures were measured with a Sensotec tensometric transducer (150 kPa resolution) and a Heise pressure gauge (70 kPa accuracy).

## RESULTS

**Equation of State.** The variation of specific volume with temperature at various pressures is shown in Figure 2. Note the small change in volume at the isotropic–cholesteric transition (I–Ch, indicated by the symbols). Also shown in Figure 2 is the volume change for the cholesteric state after subtraction of a linear extrapolation of the isotropic volume data. This emphasizes the abrupt decrease in volume on cooling, which identifies the I–Ch transition. For the two highest pressures (150 and 170 MPa), there follows immediately a larger, more gradual decrease in volume due to crystallization (three-dimensionally ordered solid phase). In the inset is a double logarithmic plot of the I–Ch transition temperature versus volume, the slope of which yields a value for the thermodynamic potential parameter:<sup>14</sup>

$$\Gamma = \frac{d \log T_{I-Ch}}{d \log V_{I-Ch}} \quad (1)$$

that is equal to  $8.1 \pm 0.3$ .

The volume data in the isotropic phase can be described by the Tait equation of state:<sup>15</sup>

$$V_I = 0.9641 \exp(6.818 \times 10^{-4} T) \times \left[ 1 - 0.894 \ln \left( 1 + \frac{P}{206.7 \exp(-0.00428T)} \right) \right] \quad (2)$$

with  $V$  in  $\text{cm}^3/\text{g}$ ,  $T$  in Celsius, and  $P$  in MPa. For the cholesteric phase, we obtain:

$$V_{Ch} = 0.9652 \exp(7.606 \times 10^{-4} T) \times \left[ 1 - 0.894 \ln \left( 1 + \frac{P}{187.2 \exp(-0.00429T)} \right) \right] \quad (3)$$

although the uncertainty is large due to the narrow temperature range over which the volume of this phase could be measured.

**Thermodynamic Transitions and Phase Diagram.** The complex dielectric permittivity,  $\epsilon^* = \epsilon' - i\epsilon''$ , was measured as a function of temperature at 0.1 MPa, and as a function of pressure at up to ca. 1 GPa at 280.0, 295.9, 319.7, and 259.3 K. Figure 3 shows dielectric loss spectra at 0.1 MPa, obtained on cooling from the isotropic phase; only a single peak is visible.

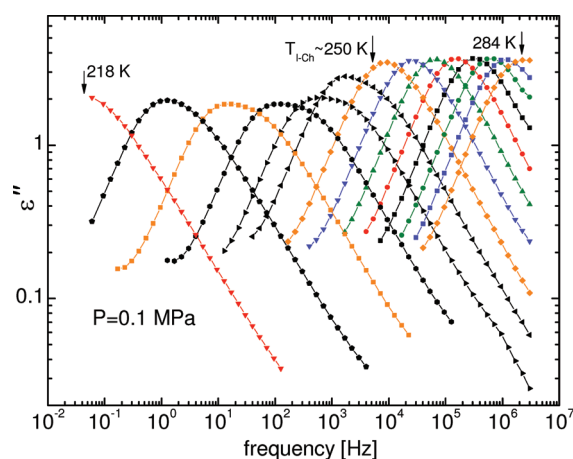


**Figure 3.** Typical dielectric spectra at various temperatures at  $P = 0.1$  MPa (decreasing  $T$ ). Crystallization does not occur, and the transition from isotropic to cholesteric is evident at about 250 K.

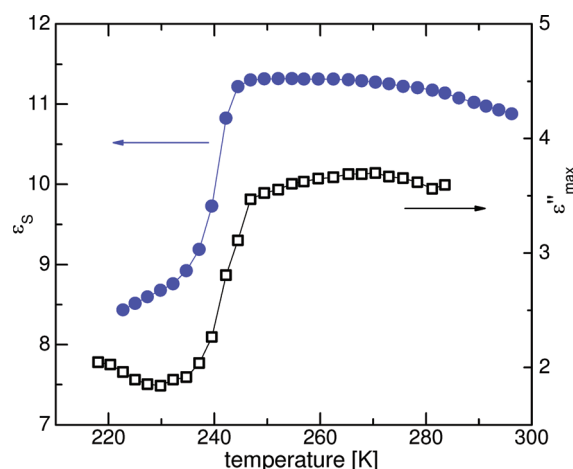


**Figure 4.** Static dielectric permittivity and peak value of dielectric loss versus temperature, with abrupt changes at the isotropic–cholesteric phase transition.

This corresponds to the  $\alpha$ -relaxation, reflecting isotropic reorientation of the  $5^*CB$  molecule. At the I–Ch transition, the  $\alpha$ -process begins to split into a double peak, with slower and faster components corresponding to the respective longitudinal (flip–flop) and transverse (spinning and/or precession) motions. The phase transition brings about marked changes in the magnitude of both the static permittivity and the maximum in the dielectric loss (Figure 4). These results are in accord with previous dielectric investigations of  $5^*CB$ .<sup>3,9,10,16</sup>

Increasing pressure slowly in the isotropic phase, crystallization occurs rather than a transition to the cholesteric phase, with a qualitatively different effect on the dielectric spectra (Figure 5). The dielectric loss rapidly decreases, with the disappearance of the  $\alpha$ -process upon crystallization. This behavior was also observed by Rzoska et al.,<sup>10</sup> who reported an I–Ch transition on cooling, and on compressing when the transition temperature was less than 265 K. For  $T > 265$  K, only crystallization of the isotropic liquid was observed, at odds with the  $PVT$  isobars in Figure 2. The latter indicate the I–Ch transition at temperatures up to ca. 300 K.

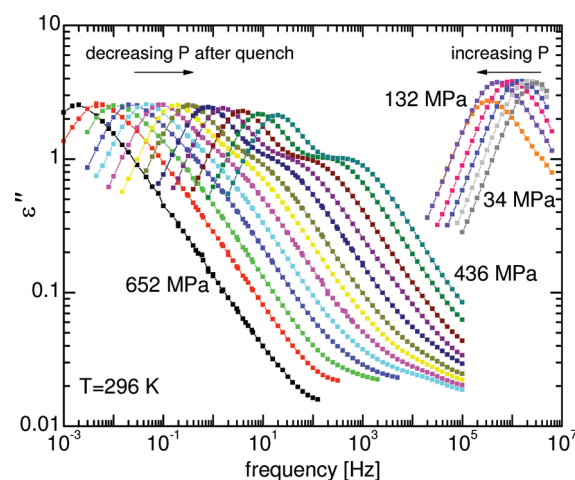


**Figure 5.** Typical dielectric spectra at various pressures along an isotherm ( $T = 296$  K), in the isotropic phase (on increasing  $P$ ) and cholesteric phase (on decreasing pressure, after remelting and pressure quenching).

The melting temperature,  $T_{m1}$ , of the solid phase of  $5^*CB$  is around 282 K at ambient pressure and increases with increasing pressure, in accord with other results.<sup>10</sup> (An estimate for the melting point at elevated pressure,  $T_m = 298$  K at  $P = 34 \pm 5$  MPa, was obtained by slowly decreasing the pressure on a previously crystallized sample, with  $T_m$  defined by an abrupt increase in the dielectric constant and loss.) Note that  $T_m$  is much higher than  $T_{I-Ch}$ ; therefore, the cholesteric phase is always metastable with respect to the solid (crystalline) phase. The difference in the phase sequence between that observed using DRS<sup>10</sup> and herein by  $PVT$  is a consequence of the different effective rates of cooling and compression. Isobaric  $PVT$  measurements employ a constant cooling rate of 2 K/min, while for DRS the sample is held at each state point for at least 30 min prior to measurement, allowing much more time for crystallization to occur. In the faster  $PVT$  experiment, the I–Ch transition transpires before crystallization occurs, whereas in the dielectric measurements crystallization proceeds before the I–Ch transition is reached.

By combining the results of the two techniques, we can construct the phase diagram (Figures 6 and 7) revised from that previously published.<sup>10</sup> In Figure 6, the transitions between metastable phases are displayed, while Figure 7 shows the actual transitions observed on cooling for the two techniques having different time scales. Note that the DRS crystallization line  $T_c(P)$  has a higher slope than  $T_{I-Ch}(P)$ , and the two lines intersect at ca. 265 K. This explains the curious behavior observed in the dielectric experiments in ref 10, wherein crystallization occurred above 265 K but not at lower  $T$ .

Starting in the isotropic state, crystallization can be circumvented by rapid application of pressure at constant temperature; the sample passes into the cholesteric state and then vitrifies. By a subsequent gradual decrease of pressure, the dynamics in the cholesteric phase can be studied in a region sufficiently close to  $T_g$ , because crystallization is very slow (time scale of hours or longer). Spectra were taken in the direction of decreasing pressure, until a low enough pressure was reached that the material crystallized. The regime where the cholesteric phase dynamics becomes inaccessible by dielectric spectroscopy due to crystallization is denoted in Figure 6 by the dashed line.

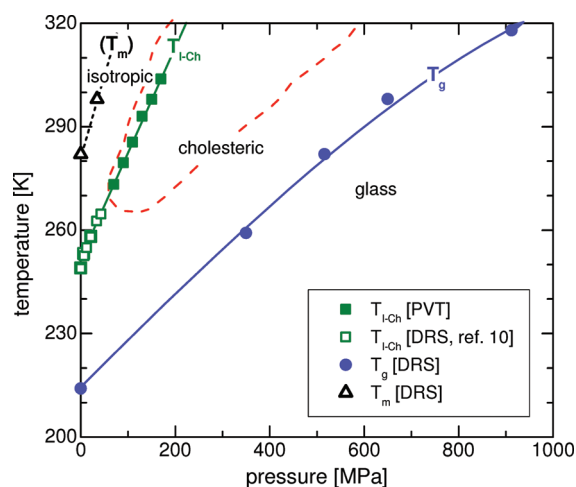


**Figure 6.**  $P$ – $T$  phase diagram of 5\*CB. At lower  $T$ /higher  $P$  than the melting line (triangles), the isotropic and cholesteric phases are metastable with respect to an ordered crystalline phase. The dashed line encloses the region where crystallization occurs on a time scale of minutes or faster, and where therefore dielectric data cannot be reliably obtained.

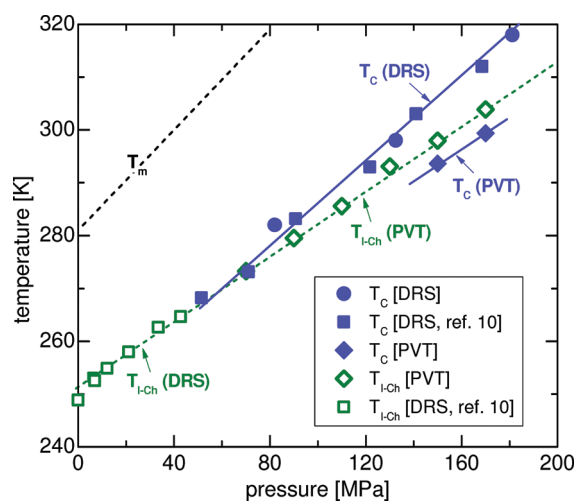


**Figure 7.** Isotropic–crystal and isotropic–cholesteric transition temperatures obtained from dielectric spectroscopy experiments at increasing pressure. Also shown are the melting line and isotropic–cholesteric transition line, the latter determined from PVT measurements. For isotherms above 265 K, crystallization occurs before the isotropic–cholesteric transition is reached due to the slower pressurization rate of the dielectric experiment.

**Dynamics.** A single loss peak, corresponding to the structural  $\alpha$ -relaxation, is observed in the isotropic phase. It was analyzed by fitting the transform of the Kohlrausch (KWW) function:<sup>17</sup>

$$\varepsilon''(\omega) = \Delta\varepsilon\omega \int_0^\infty \varepsilon(t) \cos(\omega t) dt \quad (4)$$

where

$$\varepsilon(t) = \exp[-(t/\tau_K)^\beta] \quad (5)$$

$\Delta\varepsilon$  is the dielectric relaxation strength,  $\omega$  is the angular frequency, and  $\beta$  is the stretching exponent ( $0 < \beta \leq 1$ , with  $\beta = 1$  corresponding to a Debye process). A power law is used to

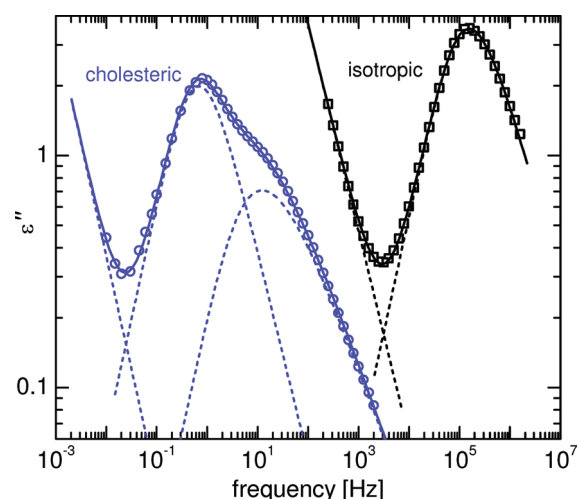


**Figure 8.** Typical fits to the dielectric spectra in the isotropic and cholesteric phases. The lines are fits to a sum of two Kohlrausch functions (eq 5), corresponding to the two relaxation processes, and a term reflecting ionic conductivity.

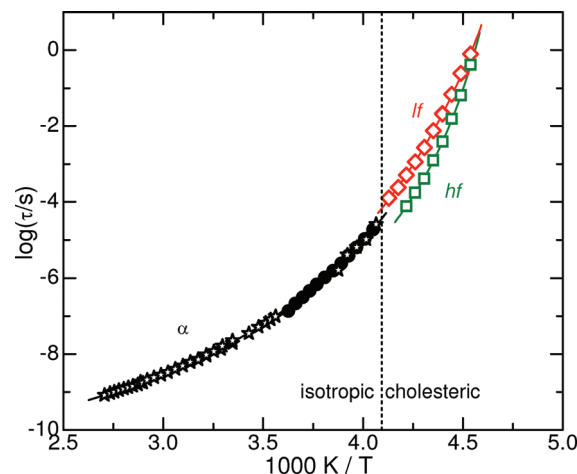


**Figure 9.** Relaxation times as a function of inverse temperature at 0.1 MPa. For the isotropic state, data ( $\star$ ) from ref 9 are also included. The lines are fits of eq 7, with the clearing temperature ( $\approx 244.3$  K) indicated by the vertical dashed line.

describe the conductivity contribution at low frequencies,  $\varepsilon'' \sim \omega^{-s}$  with  $0.9 \leq s \leq 1$ . The Kohlrausch relaxation time,  $\tau_K$ , is related to the  $\tau_\alpha$  defined as the inverse of the frequency of the peak maximum according to the empirical equation:<sup>18</sup>

$$\tau_\alpha \approx (0.175\beta^2 + 0.266\beta + 0.560)\tau_K \quad (6)$$

The spectra in the cholesteric phase were fit by a sum of two Kohlrausch functions, corresponding to the two relaxation processes, and a conductivity term. Figure 8 shows typical fits to the spectra in the isotropic and cholesteric states. The relaxation times of the three processes (labeled  $\alpha$ , lf, and hf) are plotted versus reciprocal  $T$  in Figure 9, for the 0.1 MPa isobar and as a function of  $P$  for the four isotherms in Figure 10.

The VFTH equation:

$$\tau(T) = \tau_\infty \exp\left(\frac{D_T T_0}{T - T_0}\right) \quad (7)$$

was fit to the isobaric relaxation times, where  $D_T T_0$  and  $\tau_\infty$  are temperature-independent. A variation of the VFTH equation<sup>19</sup> was used to describe the isothermal data:

$$\tau(P) = \tau_0 \exp\left(\frac{D_P P}{P_0 - P}\right) \quad (8)$$

where  $P_0$  is independent of pressure,  $D_P$  is a pressure-independent constant, and  $\tau_0$  is  $\tau(T)$  from eq 7 at the temperature of the isotherm. The parameters for eqs 7 and 8 are listed in Table 1. From these, we can calculate the fragility,  $m \equiv ((d \log(\tau))/(d(T_g/T)))|_{T=T_g} = D_T((T_0 T_g)/(T_g - T_0)^2)$ , equal to 88 at  $P = 0.1$  MPa using  $T_g(\tau_\alpha = 10^2 \text{ s}) = 214.5 \text{ K}$ . This is substantially larger than the nearly Arrhenius value for 5CB,  $m \sim 16$ .<sup>3</sup>

**Dynamics in the Isotropic Phase.** The  $\alpha$  process in the isotropic state is well described by the KWW function, with the  $\beta$  increasing (narrower peak) for higher temperature or lower pressure (Figure 11). However, for a given  $\tau_\alpha$ ,  $\beta$  is approximately constant, independent of thermodynamic conditions. This property of isochronal superposition is known for many nonmesogenic molecular liquids and polymers.<sup>20,21</sup>

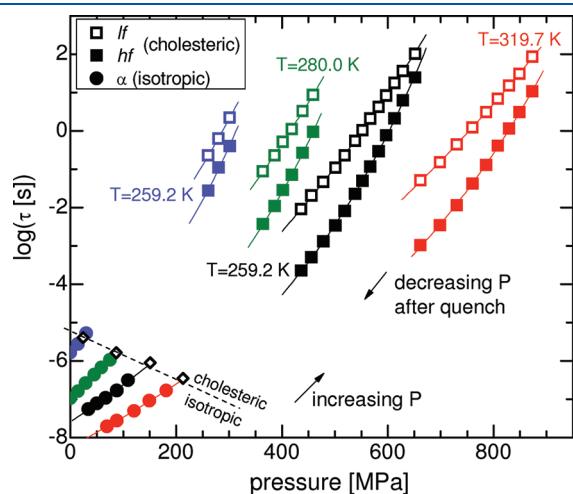


**Figure 10.** Relaxation times as a function of pressure for the four isotherms. The lines are fits of eq 8.

Another common property of nonassociated liquids and polymers is conformance of the relaxation time to the scaling law:<sup>12,22</sup>

$$\tau = f(TV^\gamma) \quad (9)$$

where  $\gamma$  is a material constant. Larger  $\gamma$  corresponds to a steeper intermolecular potential and implies a greater contribution of volume, relative to that of temperature, to the dynamics.

Equation 9 has also been found to hold for the longitudinal relaxation time in the nematic and smectic phases of liquid crystals.<sup>13,22,23</sup> In this case, the scaling exponent  $\gamma_{||}$  is approximately equal to the thermodynamic potential parameter for the clearing (nematic–isotropic or smectic–isotropic) transition. This implies that the longitudinal relaxation time at the clearing point (approached from the low-temperature side) must be constant, independent of thermodynamic conditions.

It is unclear whether this equivalence of  $\gamma_{||}$  and  $\Gamma$  and the invariance of  $\tau$  at the clearing point are maintained when the transition is approached from the high-temperature side. In general, the dynamic scaling exponents  $\gamma_{||}$  for longitudinal relaxation in the liquid crystal state and  $\gamma$  for the isotropic  $\alpha$  relaxation are not necessarily equal; the former reflects the

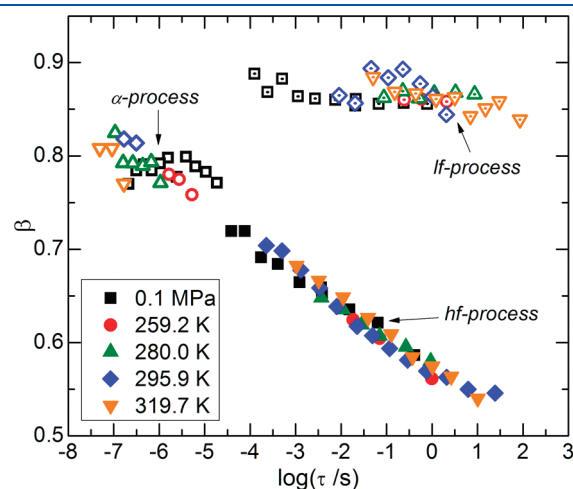


**Figure 11.** Stretching exponent for the  $\alpha$ , hf, and lf processes as a function of their respective relaxation times. The hf process seems to continue the same  $\beta(\tau)$  dependence as the isotropic  $\alpha$ .

**Table 1.** Fitting Parameters (Eqs 7 and 8) for Relaxation Spectra in Isotropic and Cholesteric Phases of 5\*CB

	cholesteric								isotropic			
	hf				lf				$\alpha$			
$T$ [K]	259.2	280.0	395.9	319.7	259.2	280.0	395.9	319.7	259.2	280.0	395.9	319.7
$\log(\tau_0/s)$	-6.14	-7.62	-8.67	-9.16	-5.59	-6.72	-7.67	-8.13	-5.78	-6.96	-7.59	-8.24
$D_P$	21.7	21.7	21.7	21.7	47.7	47.7	47.7	47.7	36.6	36.6	36.6	36.6
$P_0$ [MPa]	795	1029	1260	1862	1354	1699	2040	2675	983	1255	1740	2140
	cholesteric								isotropic			
	hf				lf				$\alpha$			
$\log(\tau_\infty/s)$	-10.5				-11.6				-11.4			
$D_T$	3.43				6.61				5.51			
$T_0$ [K]	192				177				182			

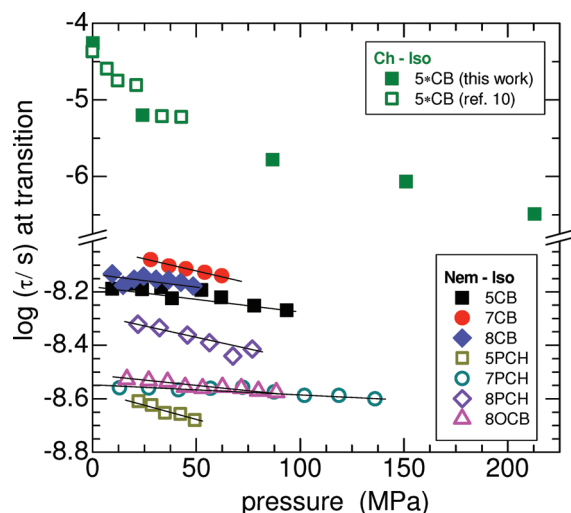


**Figure 12.** Isotropic relaxation time at the clearing point (note scale break).

steepness of the intermolecular potential in the preferred orientation adopted by the mesogenic molecules, whereas the latter averages over all orientations. Additionally,  $\Gamma$  can be different on the low- and high-temperature sides of the clearing transition, if the volume change at the transition is large, for example, as found for smectic liquid crystals. (We calculate  $\Gamma$  from volumes on the high-temperatures side of the transition when comparing to  $\gamma$ , and from the low-temperature side for comparisons to  $\gamma_{||}$ .)

For most liquid crystals, the isotropic relaxation process at the clearing point is in the GHz range and is thus not readily accessible by high-pressure relaxation measurements. This means the scaling analysis requires extrapolation, which limits the accuracy of determinations of scaling exponents  $\gamma$ . However, the equality  $\gamma = \Gamma$  can be assessed directly from the value of the relaxation time at the clearing point. Literature results<sup>24–30</sup> for  $\tau_{\alpha}$  in the isotropic phase at the isotropic–nematic transition of the liquid crystals  $n$ CB and  $n$ PCH ( $n = 5, 7, 8$ ) and SOCB are collected in Figure 12. Up to pressures around 100 MPa,  $\tau_{\alpha}$  at the clearing point is essentially constant, with only a modest tendency to decrease with increasing pressure. In contrast,  $5^*CB$  behaves very differently;  $\tau_{\alpha}$  changes by orders of magnitude at the clearing point (Figure 12).

In Figure 13, we plot the  $\alpha$  relaxation times against the scaling variable  $TV^{\gamma}$  for  $5^*CB$ ; the value  $\gamma = 3.7$  superimposes all points onto a master curve. Although density scaling holds quite accurately, this exponent is much smaller than the  $\Gamma = 8.1$  obtained for the thermodynamic phase transition (see Figure 2). This is consistent with the large change of  $\tau_{\alpha}$  with pressure at the transition point.

It is worth noting that for the liquid crystals in Figure 12 other than  $5^*CB$ , the clearing transition occurs for relaxation times on the order of  $10^{-9}$ – $10^{-8}$  s, which is shorter than  $\tau$  at the dynamic crossover for most supercooled liquids.<sup>31</sup> When  $\tau$  is small, its temperature and volume dependences are weak. In contrast, the Ch–I transition in  $5^*CB$  transpires deep in the supercooled state, where relaxation times are much more sensitive to pressure and temperature. As a consequence, the relaxation time at the clearing point is substantially more sensitive to pressure for  $5^*CB$  than for the other liquid crystals of Figure 12. Possibly also underlying the observed variation with  $P$  of  $\tau$  in Figure 12 is the

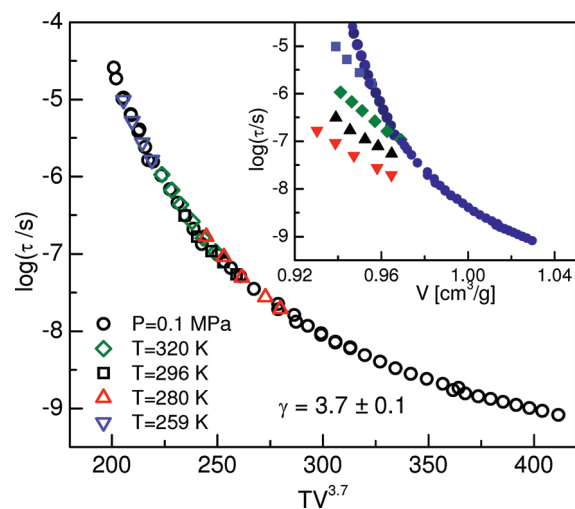


**Figure 13.** Density scaling in isotropic phase.

fact that the Ch–I transition in  $5^*CB$  involves metastable phases, whereas for the other cases both phases are thermodynamically stable.

It is interesting to compare the dynamics at the clearing point of  $5^*CB$  with the dynamics at the melting point of nonmesogenic liquids. The temperature and volume dependence of the melting transition can be characterized by a scaling exponent  $\Gamma_m = d \log V_m / d \log T_m$ , analogous to the thermodynamic potential parameter. For rigid, nonpolar spherical molecules,  $\Gamma_m$  is equal to the density scaling exponent  $\gamma$  for the dynamics, whereas for liquids with a nonspherical molecular shape, internal degrees of freedom, or strong internal dipole moments, the two exponents are different.<sup>32</sup> In the latter, more general situation, the dynamics is more sensitive to volume than to the melting point (i.e.,  $\gamma > \Gamma_m$ ), opposite to the behavior observed for the clearing point of  $5^*CB$ .

**Dynamics in the Cholesteric Phase.** In the cholesteric phase, dielectric relaxation occurs via two processes, slow rotation around the short axis and faster spinning or precession about the long axis. (As in Figure 9, we label the lower frequency, longitudinal motion “lf” and the faster transverse relaxation “hf”.)  $\tau_{lf}$  is generally 1–2 orders of magnitude longer than  $\tau_{hf}$ . As was the case for the isotropic  $\alpha$  relaxation, both of these mesophase relaxations have strongly non-Arrhenius temperature and non-linear pressure dependences.

Figure 14 shows the relaxation times plotted versus specific volume, with the usual wide variations in behavior, because  $V$  is not the control parameter governing the dynamics. In the inset to this figure, the  $\tau$  values measured as a function of  $T$  at elevated pressures are replotted versus the scaling variable  $TV^{\gamma}$ . The need of extrapolating eq 3 reduces the accuracy of the superpositioning (and the ambient pressure data are omitted entirely because of the overly long extrapolation required); nevertheless, the relaxation times for the cholesteric state conform reasonably well to eq 9. Notwithstanding the uncertainty in the scaling exponents for the hf and lf processes, both are significantly lower than the thermodynamic potential parameter for the clearing point; in this respect,  $5^*CB$  deviates from the general behavior of  $\gamma_{lf} \approx \Gamma$  found for a large number of liquid crystals.

The lf process has a stretching exponent  $\beta \approx 0.9$  independent of thermodynamic conditions; that is, it is almost Debye-like with a temperature- and pressure-independent shape. Similar behavior has been observed in other liquid crystal phases: In the

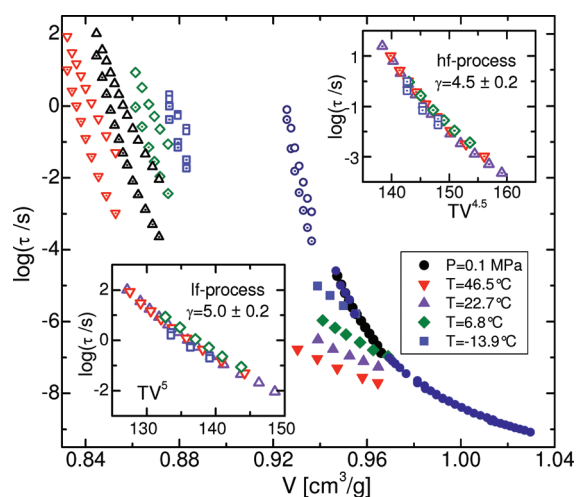


**Figure 14.** Relaxation times versus volume: isotropic phase (filled symbols); cholesteric phase (open and dotted symbols). The insets show scaling plots of  $\tau$  for the cholesteric phase (omitting the ambient pressure  $\tau$ , due to the overly long extrapolation of the equation of state).

supercooled nematic phase of the liquid crystal mixture E7, similar to 5\*CB, a quasi-Debye longitudinal relaxation and broader tumbling mode are present, the latter having more Arrhenius-like behavior (i.e., larger  $D_T$  in eq 7), with the two processes merging on approach to  $T_g$ .<sup>33</sup> Likewise, in 5\*CB, the hf process is broader, and the peak breadth increases with proximity to the glass transition. These  $\beta$  are plotted in Figure 11, where it can be seen that the cholesteric hf and isotropic  $\alpha$  relaxations follow similar  $T$ -dependences, despite the discontinuities in the relaxation strength (Figure 4) and the relaxation time (Figure 9) at the Ch–I transition.

The hf process corresponds to a distribution of relaxation times caused by different motions occurring over the same time scale, for example, reorientation about the long axis and internal rotations of parts the molecule, as well as various “crankshaft-type” motions within the alkyl tails (which are weakly polar).<sup>34</sup> This faster, smaller-scale process has the characteristics of cooperative relaxation (non-Arrhenius relaxation and stretched exponential relaxation), and thus the lf process must also be cooperative: the longitudinal motions require free space be created via displacement of neighboring molecules (rotation–translation coupling).<sup>13</sup>

Analogous behavior is observed in other classes of materials, such as relaxation of large polar probes in viscous liquids<sup>35</sup> and the slow relaxation in monoalcohols.<sup>36</sup> In both cases, a slow Debye-like relaxation that approximately follows the temperature dependence of the  $\alpha$  process is observed. The Debye nature of the slow process is the result of averaging; on the time scale of the slow process, the fast process (to which it is coupled) occurs many times. Therefore, the slow process senses only an average relaxation, or “local viscosity”, and thus relaxes exponentially. This is analogous to reorientation of a rigid object in a viscous medium, described in the original Debye model.<sup>37</sup>

For both relaxations in the cholesteric phase, the shape of the dielectric loss peak (described by the stretching exponent  $\beta$ , Figure 11) depends only on the relaxation time, independent of thermodynamic conditions. However, this cannot be true of the overall spectrum, given their different  $T$ - and  $P$ -dependences. Figure 15 shows spectra at different state points selected such that  $\tau_{lf}$  is constant. It is evident that for a given peak frequency,

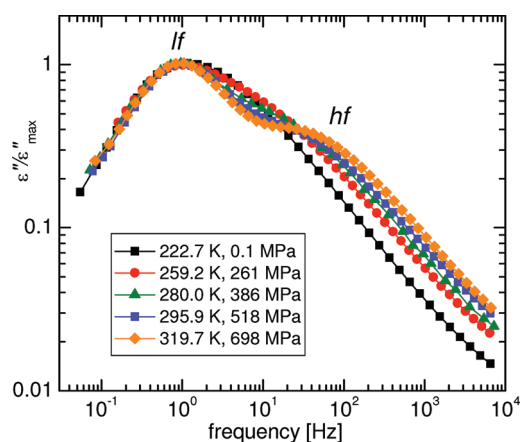


**Figure 15.** Scaled dielectric spectra in cholesteric phase. For a given  $\tau_{lf}$  the hf and lf processes become increasingly separated with increasing temperature and pressure.

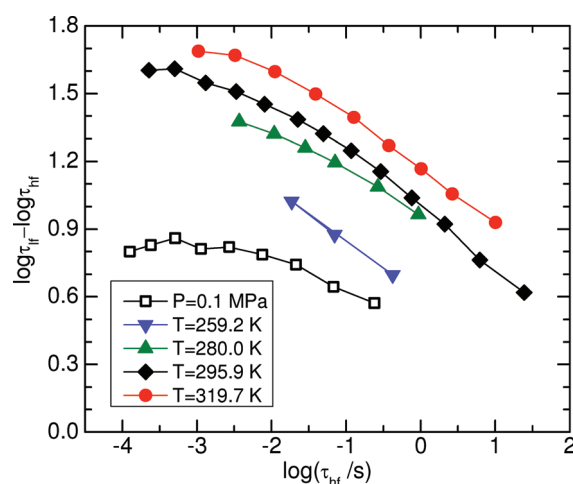


**Figure 16.** Separation in decades between the relaxation times of the hf and lf processes in the cholesteric phase.

the separation between the two peaks increases with increasing pressure and temperature. This is more evident in Figure 16, which shows  $\log(\tau_{lf}/\tau_{hf})$  as a function of the  $\tau_{hf}$ . Additionally, the two relaxations become closer on approach to  $T_g$  by cooling or compressing. The fact that the separation of the peaks is not constant for given  $\tau$  indicates that these processes cannot have the same scaling exponent  $\gamma$ , consistent with Figure 14.

**Effect of dc Bias on Relaxation.** Figure 17 shows the effect of applying a dc electric field on the dielectric spectrum in the cholesteric phase at ambient pressure and  $-45^\circ\text{C}$ . The relaxation times of the two processes remain constant; however, their intensities are affected by the static field. The intensity of the lower frequency relaxation increases substantially, tending to a value almost 3-fold higher than in the absence of a bias voltage. The higher frequency process, on the other hand, becomes weaker, but the change is small. Although the mechanism for these electric field effects in 5\*CB is unclear, such behavior is often observed with chiral structures, wherein a sufficiently strong electric or magnetic field can unwind the helix. Chiral N\* and smectic C\* phases can be converted to well-oriented nematic or smectic C phases, which increases the dielectric permittivity.

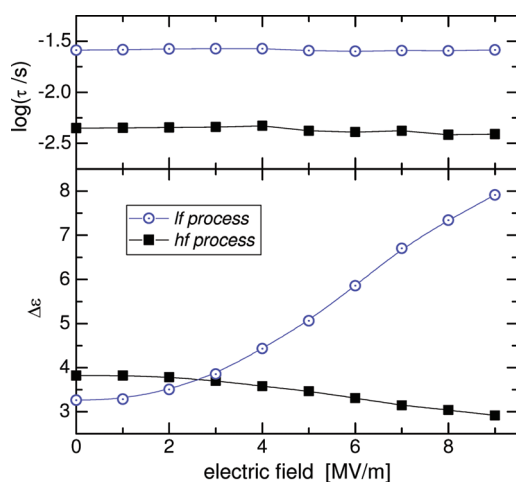


**Figure 17.** Effect of static electric field on relaxation times and strength in the cholesteric phase ( $P = 0.1$  MPa,  $T = -45$  °C).

## SUMMARY

PVT and dielectric spectroscopy measurements over a range of temperature, pressure, and frequency broaden our understanding of the phase diagram and dynamical properties of 5\*CB. The metastable cholesteric phase could be attained by an isobaric decrease of temperature or an isothermal increase of pressure. In the available frequency range a single relaxation was observed in the isotropic phase, whereas in the cholesteric phase two processes were evident. The lower frequency process corresponds to longitudinal (flip–flop) motions. Precession and/or spinning motions contribute to the higher frequency response in the chiral phase. All relaxation times exhibit nonlinear dependences on pressure and temperature. The data conform to thermodynamic scaling, with the obtained potential parameters characterizing the steepness of the interaction potential. These were compared to those determined for other liquid crystals and glass-forming liquids.

## AUTHOR INFORMATION

### Corresponding Author

\*E-mail: mike.roland@nrl.navy.mil.

### Present Addresses

<sup>†</sup>i\_SW Corp., Arlington, Virginia 22203, United States.

<sup>‡</sup>Faculty of Physics and Applied Computer Science, AGH University of Science and Technology, Mickiewicza 30, 30-059 Kraków, Poland.

## ACKNOWLEDGMENT

The work at NRL was supported by the Office of Naval Research. D.F. and R.B.B. acknowledge respective National Research Council and American Association of Engineering Education postdoctoral appointments.

## REFERENCES

- (1) Gray, G. W.; Harrison, K. J.; Nash, J. A. *Electron. Lett.* **1973**, *9*, 130.
- (2) Gray, G. W.; McDonnell, D. G. *Mol. Cryst. Liq. Cryst.* **1976**, *37*, 189.
- (3) Massalska-Arodz, M.; Williams, G.; Smith, I.; Conolly, Ch.; Aldridge, G. A.; Dabrowski, R. *J. Chem. Soc., Faraday Trans.* **1998**, *94*, 387.
- (4) Mayer, J.; Witko, W.; Massalska-Arodz, M.; Williams, G.; Dabrowski, R. *Phase Trans.* **1999**, *69*, 199.

- (5) Witko, W.; Sciesinski, J.; Sciesinska, E.; Massalska-Arodz, M.; Mayer, J.; Dabrowski, R. *Mol. Cryst. Liq. Cryst.* **1999**, *330*, 391.
- (6) Suzuki, H.; Inaba, A.; Krawczyk, J.; Massalska-Arodz, M. *J. Chem. Thermodyn.* **2008**, *40*, 1232.
- (7) Inaba, A.; Suzuki, H.; Krawczyk, J.; Massalska-Arodz, M. *Chem. Phys. Lett.* **2008**, *463*, 90.
- (8) Suzuki, H.; Inaba, A.; Krawczyk, J.; Massalska-Arodz, M.; Kikuchi, T.; Yamamuro, O. *J. Non-Cryst. Solids* **2011**, *357*, 734.
- (9) Urban, S.; Gestblom, B.; Dabrowski, R. *Phys. Chem. Chem. Phys.* **1999**, *1*, 4843.
- (10) Rzoska, S. J.; Paluch, M.; Pawlus, S.; Drozd-Rzoska, A.; Zioło, J.; Jadżyn, J.; Czupryński, K.; Dabrowski, R. *Phys. Rev. E* **2003**, *68*, 031705.
- (11) Ferry, J. D. *Viscoelastic Properties of Polymers*, 3rd ed.; Wiley: New York, 1980.
- (12) Roland, C. M.; Hensel-Bielowka, S.; Paluch, M.; Casalini, R. *Rep. Prog. Phys.* **2005**, *68*, 1405.
- (13) Urban, S.; Roland, C. M. *J. Non-Cryst. Solids* **2011**, *357*, 740.
- (14) Chandrasekhar, S. *Liquid Crystals*, 2nd ed.; Cambridge University Press: Cambridge, UK, 1993.
- (15) Zoller, P.; Walsh, D. J. *Standard Pressure-Vol.-Temperature Data for Polymers*; Technomic: Lancaster, PA, 1995.
- (16) Mayer, J.; Massalska-Arodz, M.; Krawczyk, J. *Mol. Cryst. Liq. Cryst.* **2001**, *366*, 211.
- (17) Kohlrausch, R. *Pogg. Ann. Phys. Chem.* **1854**, *91*, 179. Williams, G.; Watts, D. C. *Trans. Faraday Soc.* **1970**, *66*, 80.
- (18) Santangelo, P. G., unpublished.
- (19) Johari, G. P.; Whalley, E. *Faraday Symp. Chem. Soc.* **1972**, *6*, 23.
- (20) Roland, C. M.; Casalini, R.; Paluch, M. *Chem. Phys. Lett.* **2003**, *367*, 259.
- (21) Ngai, K. L.; Casalini, R.; Capaccioli, S.; Paluch, M.; Roland, C. M. *J. Phys. Chem. B* **2005**, *109*, 17356.
- (22) Roland, C. M. *Macromolecules* **2010**, *43*, 7875.
- (23) Roland, C. M. *Soft Matter* **2008**, *4*, 2316.
- (24) Wuerflinger, A. *Int. Rev. Phys. Chem.* **1993**, *12*, 89.
- (25) Brueckert, T.; Wuerflinger, A. *Ber. Bunsen-Ges. Phys. Chem.* **1993**, *97*, 1209.
- (26) Urban, S.; Wuerflinger, A. *Adv. Chem. Phys.* **1997**, *98*, 143.
- (27) Brueckert, T.; Buesing, D.; Wuerflinger, A.; Urban, S. *Mol. Cryst. Liq. Cryst.* **1995**, *262*, 209.
- (28) Brueckert, T. Doctoral Thesis, Ruhr-University Bochum, Bochum, Germany, 1996.
- (29) Urban, S.; Buesing, D.; Wuerflinger, A.; Gestblom, B. *Liq. Cryst.* **1998**, *25*, 253.
- (30) Brueckert, T.; Urban, S.; Wuerflinger, A. *Ber. Bunsen-Ges. Phys. Chem.* **1996**, *100*, 1133.
- (31) Roland, C. M.; Casalini, R. *J. Non-Cryst. Solids* **2005**, *351*, 2581.
- (32) Fragiadakis, D.; Roland, C. M. *Phys. Rev. E* **2011**, *83*, 031504.
- (33) Brás, A. R.; Dionisio, M.; Huth, H.; Schick, Ch.; Schönhals, A. *Phys. Rev. E* **2007**, *75*, 061708.
- (34) Zajac, W.; Urban, S.; Domenici, V.; Geppi, M.; Veracini, C. A.; Telling, M. T. F.; Gabrys, B. *J. Phys. Rev. E* **2006**, *73*, 051704.
- (35) Huang, W.; Richert, R. *Philos. Mag.* **2007**, *87*, 371.
- (36) Fragiadakis, D.; Roland, C. M.; Casalini, R. *J. Chem. Phys.* **2010**, *132*, 144505.
- (37) Debye, P. *Polar Molecules*; Dover: New York, 1928.